IEEE Access
Multidisciplinary | Rapid Review | Open Access Journal

Received December 26, 2019, accepted January 12, 2020, date of publication January 24, 2020, date of current version February 17, 2020.

Digital Object Identifier 10.1109/ACCESS.2020.2969228

The Measurement Method for the Size of the Hole on the Part Surface Based on Grating Image Processing

YONG JIN[1], YIMIN CHANG[1], JIAYING WANG[2], MAOZHEN LI[1,3], LIHENG REN[1], AND YOUXING CHEN[1]

[1]School of Information and Communication Engineering, North University of China, Taiyuan 030051, China
[2]School of Electrical Engineering and Telecommunications, University of New South Wales, Sydney, NSW 2052, Australia
[3]Department of Electronic and Computer Engineering, Brunel University London, Uxbridge UB8 3PH, U.K.

Correspondence author: Maozhen Li (nuclimaozhen@163.com)

This work was supported in part by the Shanxi Scholarship Council of China under Grant 2016–084, and in part by the Shanxi Province Natural Science Foundation under Grant 201901D111155.

ABSTRACT With the development of manufacturing industry, the high precision size measurement for the holes on the surface of mechanical parts is required. A method for measuring size of the hole based on double projection is proposed in this paper. The CCD camera separately collects grating images which projected onto the part surface in two directions. The phase-shift method is used to calculate the phase of grating images in two directions, and the reconstructed three-dimensional shapes in the two directions are merged to measure the hole dimension. Experiment results show that the measurement accuracy of the thickness is 0.04mm, and the hole size can reach to 0.1 mm.

INDEX TERMS Grating projection, image processing, 3D reconstruction, hole size.

I. INTRODUCTION

The structure of mounting hole is necessary in all kinds of mechanical parts. The accurate measurement of hole size plays an important role in machining and assembly. Grating projection is one of the methods to realize the inspection of the holes and obtain the thickness of steel plate or part without contact. Liu *et al.* [1] used grating projection method to detect the thickness and holes of steel plate, projecting the grating onto the surface of steel plate, and solving the grating phase by wavelet transform. However, when the method is used for the measurement of deep holes, the shadow area is formed due to the occlusion of the edge of the holes, which leads to the interruption of the grating, and the shadow area cannot be reconstructed accurately. In addition, neither the noise is effectively suppressed nor the local phase information be accurately obtained by the wavelet transform method, so that the size of reconstruction accuracy for the hole is lower.

In recent years, the grating projection three-dimensional detection technology has been applied to the reconstruction of part topography and measurement of dimensions due to its high detection sensitivity and high speed. The three-dimensional morphology of the rail was accurately reconstructed by Fourier transform profilometry to achieve the detection of surface defects [2], [3]. The Fourier transform was utilized to extract the phase information of the glass surface, thereby detecting the glass defects and judging the size, position and type of the defects [4]. Zhang *et al.* [5], [6] realized the three-dimensional reconstruction of large-size objects by the Fourier transform of more image such as the wheel surface of the emu, and identified the surface defects of the wheels simultaneously. Due to the confusion of frequency, leakage and fence effect, the Fourier transform method is easy to ignore the detailed information of the shape of the object to be measured under the interference of noise, which is difficult to apply to the occasions with high precision requirements [7]–[9]. The phase shift method can accurately extract the phase information of the measured object in phase extraction. The method has been applied to extract phase information of the grating images to complete the three-dimensional reconstruction of the solder paste [10], [11]. Li *et al.* [12] extracted the phase information of the wheel by the phase shift method to achieve wheel contour reconstruction and wheel tread wear and surface defects were accurately detected. The current phase shift algorithms are: standard N-step phase shift method or equal interval

The associate editor coordinating the review of this manuscript and approving it for publication was Yonghong Peng.

full-cycle method [13], N-frame average algorithm [14], N + 1 step phase shift algorithm [15], and arbitrary equal step phase shift algorithm [16]. The stability and error response of each algorithm are different, so the choice of phase shift algorithm has an important impact on the phase calculation and subsequent 3D reconstruction accuracy [17]. The standard N-frame phase shift algorithm has the best suppression effect on the random noise of the system and is insensitive to harmonic errors below the N−1th order. It has become the most widely used phase shift algorithm in structured light measurement technology [18]. The 3-step phase shift method is the lowest-precision phase-shifting contouring method among all the phase-shifting contouring methods. Compared with the 3-step phase-shifting contouring method, the 4-step phase-shifting method can eliminate even harmonics with higher accuracy. Phase shift profiling with more phase shifts, such as 6-step phase-shift profiling, 7-step phase-shift profiling, etc. Compared to 4-step phase-shift profiling, its accuracy is limited, but the amount of calculation is increased. Therefore, 4-step phase-shifting contouring is currently the most commonly used phase-shifting contouring [19], and is also used in this paper. Due to the influence of the projection dead zone, this method still cannot accurately reconstruct the three-dimensional shape of the hole. In this paper, the reconstruction data fusion is achieved by positioning the projection blind zone, and finally the three-dimensional shape of the hole is obtained [20].

Based on the grating projection, this paper proposes a double projections part appearance quality inspection method to achieve accurate detection of part thickness and holes. In this method, the grating is projected onto the surface of part in two directions, and the surface grating images in the two directions are collected by CCD. The phase-shift method is used to solve the phase of the two directions, and the reconstructed three-dimensional morphology is fused to realize the accurate measurement of part thickness and holes.

II. DETECTION METHOD AND PRINCIPLE

The schematic diagram of the grating projection measurement system is as follows:

As shown in the figure 1, point C is the optical center of the industrial camera, and point P is the optical center of the digital projector. The distance between point C and point D is d, and the distance between them and the reference plane is l. In addition, H represents any point on the part surface and HH' is perpendicular to the reference plane and intersects with the reference plane at point H′. $\overline{HH'}$ is the distance between point H and point H′. $\overline{BA}$ is the distance between point B and point A.

Figure 1 shows that: $\Delta ABH \sim \Delta PCH$, then the following proportional relationship can be obtained:

$$\frac{d}{\overline{BA}} = \frac{l - \overline{HH'}}{\overline{HH'}} = \frac{l}{\overline{HH'}} - 1 \tag{1}$$

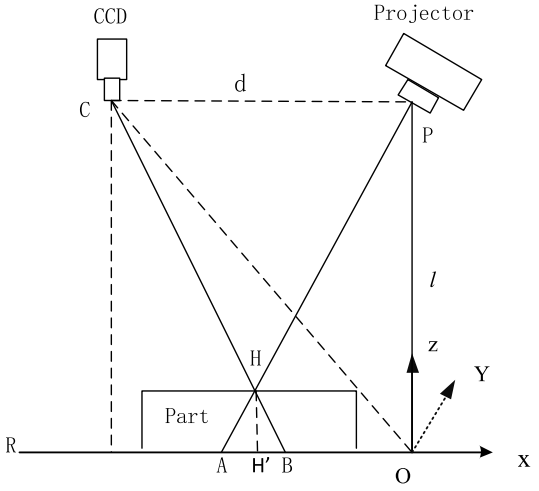

FIGURE 1. The schematic diagram of the grating projection measurement system.

The height distribution $h(x, y)$ can be expressed as:

$$h(x, y) = \overline{HH'} = \frac{l\overline{BA}}{d + \overline{BA}} \tag{2}$$

According to the structural analysis of the grating projection measurement system, the phase difference between point A and point B is related to the distance between point A and point B on the reference surface:

$$\Delta\phi(x, y) = \phi_A(x, y) - \phi_B(x, y) = 2\pi f_0 \overline{BA} \tag{3}$$

In this way, the relation between the height distribution h of the measured object and the modulation phase $\Delta\phi(x, y)$ can be obtained:

$$h = \frac{l\Delta\phi(x, y)}{\Delta\phi(x, y) + 2\pi f_0 d} \tag{4}$$

Among them, $\Delta\varphi(x, y)$ is expressed as the phase difference between the phase distribution of the measurement object surface and the phase distribution of the reference plane, and f_0 is the pitch of the grating stripes.

The method for detecting the holes of the part proposed in this paper is shown in Fig. 2. A digital projector 1, a CCD camera and a digital projector 2 are arranged at equal intervals above the steel plate. The digital light projector alternately projects equally spaced bright and dark grating fields. The CCD camera separately collects the grating image on the surface of the part, and reconstructs the same part area projected in the left and right directions in three dimensions. After reconstruction data fusion, the three-dimensional shape of the part surface is obtained.

III. ACQUISITION AND PREPROCESSING OF GRATING IMAGES

The grating image acquisition system is shown in Fig 3. In this experiment, the image of the grating on the surface of the part was acquired by oblique projection and vertical

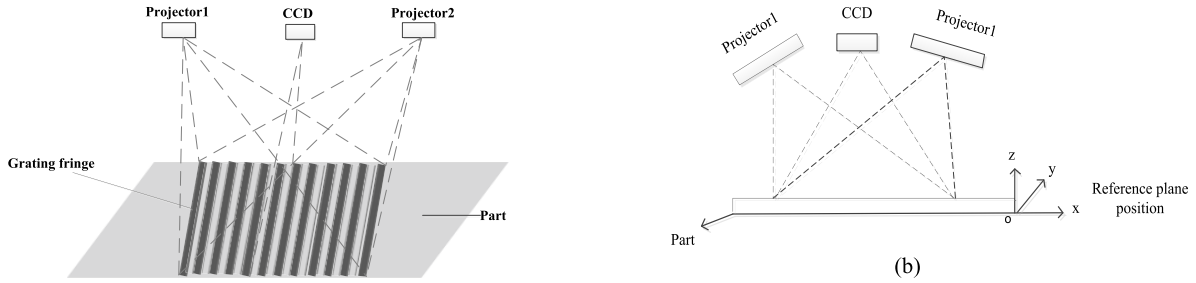

FIGURE 2. Imaging method of holes detection based on double projection: (a) the whole design of the imaging method proposed in this paper; (b) side view of (a).

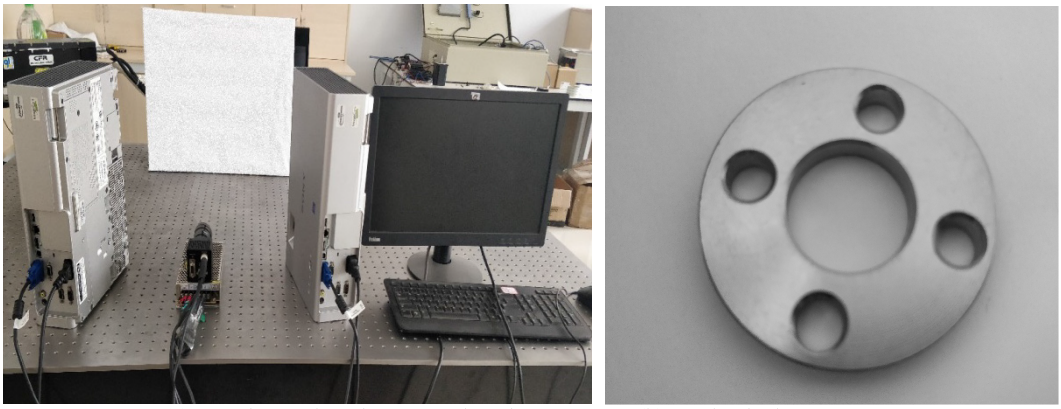

(a)Experimental equipment and environment (b) mechanical parts

FIGURE 3. Experimental equipment and environment.

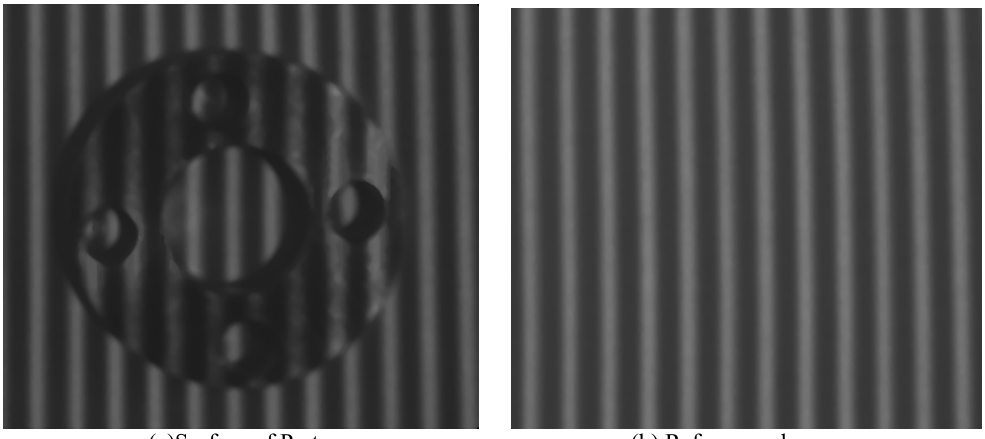

(a)Surface of Part (b) Reference plane

FIGURE 4. Images of grating fringes.

shooting. The horizontal resolution of the CCD camera was 3296 pixels and the vertical resolution was 2472 pixels. The resolution ratio of the projector was 1280 × 800 pixels.

The ratio of the grating images acquired by the CCD to the actual grating images is 10:1. The resolution ratios of all of the images are 0.1 × 0.1 mm/pixel. The distance between the CCD and the digital projector is 300 mm, and the distance between the CCD and the reference plane is 500 mm. The angle between the digital projector's optical path and the CCD optical path is 30 degrees. The digital light projector alternately projects a sinusoidal grating whose initial phase values are 0, $\frac{\pi}{2}$, π, $\frac{3\pi}{2}$ to the surface of the part to be tested, and the CCD camera collects the corresponding grating image, as shown in Fig. 4.

As can be seen from the above figure, although the digital light projector projects a standard sinusoidal grating pattern,

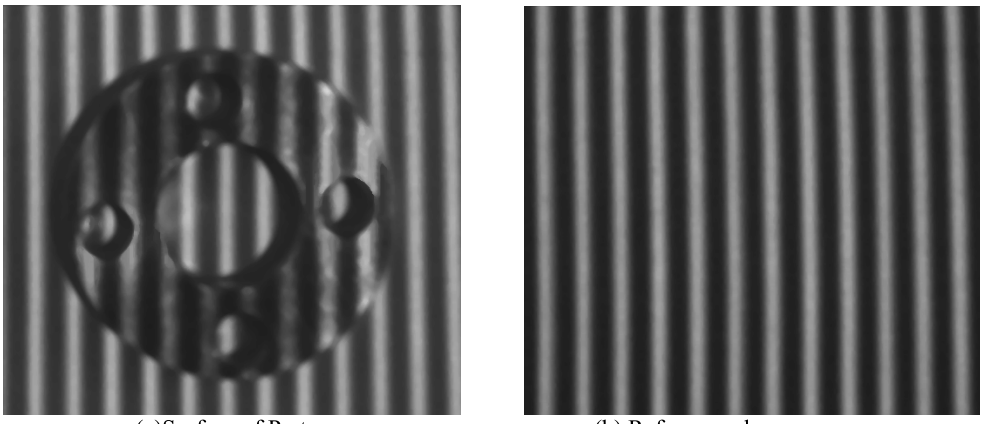

(a)Surface of Part (b) Reference plane

FIGURE 5. Rectified images of grating fringes.

due to uneven distribution of background light intensity and different reflectivity of the part surface, the grating pattern after the CCD camera has been produced has a significant difference from the standard sinusoidal grating. If the grating is not processed, the three-dimensional shape of the reconstructed part will have a large error with its original shape. In order to solve this problem, the grating image collected by CCD camera is rectified based on cosine curve in this paper to improve the accuracy of 3d reconstruction.

The ideal grating image curve can be expressed as: $I_i(\mathrm{x}) = A + B\cos(Cx)$, where i is the number of rows of grating, A, B, and C are pending coefficients. Before the correction starts, collect 100 lines of defect-free grating image curves to find the mean $I'(x)$ of the 100 lines of grating image curves. A can be determined through $A = \sum_{x=1}^{M} I'(x)$, where M is the number of columns of the grating image, B is the average of the amplitude of the grating image, and C is the frequency of the grating image. From the above, the correction coefficient is $K = I(x)/I'(x)$, multiplying each line of the captured grating image curve by the correction coefficient K, the corrected grating image curve can be obtained, as shown in Fig. 3.

IV. PHASE SOLUTION AND UNWRAPPING OF GRATING IMAGES

N grating fields with different phases are projected onto the surface of the part. The grating is deformed due to the height modulation of the part, and the image of the surface deformation grating of the part collected by the CCD camera can be expressed as:

$$I_k(x,y) = a(x,y) + b(x,y) \times \cos[2\pi f_0 x + \varphi(x,y) + (k-1) \times \frac{2\pi}{N}] \quad (5)$$

where $k = 1, 2, 3 \ldots N$, $a(x, y)$ represents the background light intensity of the grating, $b(x, y)$ represents the uneven reflectivity of the part, f_0 represents the frequency of the grating fringe, and $\varphi(x, y)$ represents the phase distribution of the surface of the part to be tested.

From the N-frame grating image represented by the above formula, $\varphi(x, y)$ can be found as:

$$\varphi(x,y) = \arctan\left\{\frac{-\sum_{k=1}^{N} I_k(x,y) \times \sin\left[\frac{2\pi}{N}(k-1)\right]}{\sum_{k=1}^{N} I_k(x,y) \times \cos\left[\frac{2\pi}{N}(k-1)\right]}\right\} \quad (6)$$

According to the above analysis, the four step phase-shift method ($N = 4$) is adopted in this paper to solve the phase. From the above formula (2), $\varphi(x, y)$ can be obtained as:

$$\varphi(x,y) = \arctan\left\{\frac{I_4 - I_2}{I_1 - I_3}\right\} \quad (7)$$

Figure 6 shows calculated wrapped phase. It can be found that the grating is interrupted due to the influence of the blind area of projection, so the shadow area cannot be accurately reconstructed.

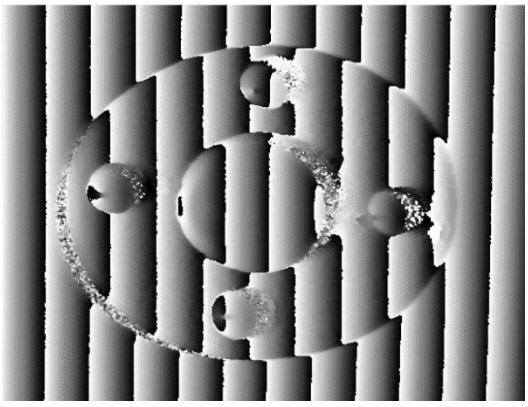

FIGURE 6. Wrapped phase maps.

Since the phase, $\varphi(x, y)$, obtained by the four step phase-shift method is calculated by the inverse trigonometric

function and the positive and negative of the numerator and denominator of formula (3), the phase distribution range is $[-\pi, \pi]$. The wrapped phase distribution is shown in figure 7. The wrapped phase needs to be unwound into an accurate and unique true phase to complete the three-dimensional reconstruction of the part.

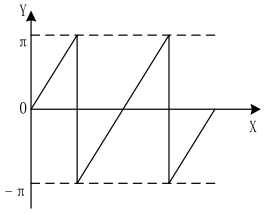

FIGURE 7. Wrapped phase.

The 3d reconstruction of parts can be completed only when the wrapped phase is unwound to the real phase. The unwrapped phase $\Phi(x, y)$ is calculated by equation (8):

$$\Phi(x, y) = \Phi(x, y) + 2n(x, y) * \pi \tag{8}$$

n(x,y) is determined by equation (9):

$$n(x, y) = \begin{cases} 0 & |\varphi(x+1, y) - \varphi(x, y)| < \pi \\ -1 & \varphi(x+1, y) - \varphi(x, y) \geq \pi \\ 1 & \varphi(x+1, y) - \varphi(x, y) \leq -\pi \end{cases} \tag{9}$$

The calculated unwrapped phase is shown in Figure 8:

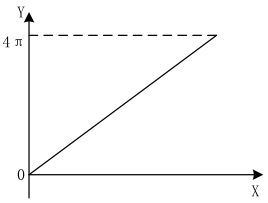

FIGURE 8. Unwrapped phase.

At present, the phase unwrapping algorithms commonly have: the branch cut algorithm, the quality-guided path following algorithm, the least-square method and so on [1]. The quality-guided path following algorithm has high precision and can accurately reconstruct the contour of the part, but the efficiency is low. Although the least-square method has high efficiency, error is heavy, and the shape of the part cannot be accurately restored. The branch cutting algorithm has the advantages of fast phase expansion operation speed and small phase error, which can meet the precision requirements of part appearance quality detection and accurately restore the three-dimensional shape of part. The 3d contour of the hole reconstructed by the unilateral projector is shown in figure 9.

V. RECONSTRUCTION OF HOLES

The four phase-shifted grating images collected by CCD camera are $I_1(i,j)$, $I_2(i,j)$, $I_3(i,j)$, $I_4(i,j)$. The grating background image can be expressed as:

$$I(i, j) = [I_1(i, j) + I_2(i, j) + I_3(i, j) + I_4(i, j)]/4 \tag{10}$$

As shown in Fig. 10, take the center circle of a part as an example, the image is binarized to obtain the position of shadow region as $II_1(i, j)$ and $II_2(i, j)$.

The reconstructed morphology of the shaded region can be expressed as:

$$\begin{cases} HA_1(i, j) = H_2(i, j) \times II_1(i, j) \\ HA_2(i, j) = H_1(i, j) \times II_2(i, j) \end{cases} \tag{11}$$

In the formula above, $nRows \leq i \leq nCols, nRows \leq j \leq nCols$, H_1 is the three-dimensional shape of the left-side projection grating fringe reconstructed part, and H_2 is the shape of the right-hand projected grating fringe reconstruction part, $II_1(i, j)$ is the location of the shaded area on the left, $II_2(i, j)$ is the location of the shaded area on the left.

After two projections, the area where the part is not affected by the shadow is *HB*, and the reconstructed contour can be expressed as:

$$\begin{cases} HB_1(i, j) = H_1(i, j) \times (1 - II_1(i, j) - II_2(i, j)) \\ HB_2(i, j) = H_2(i, j) \times (1 - II_1(i, j) - II_2(i, j)) \end{cases} \tag{12}$$

Data points in areas HB_1 and HB_2 are concentrated and divided them into two sets according to the threshold value:

$$\begin{cases} HB(i, j) \in L_1, & HB(i, j) \geq k \\ HB(i, j) \in L_2, & HB(i, j) < k \end{cases} \tag{13}$$

$$k = (\min(HB_t) + \max(HB_t))/2 \tag{14}$$

In the formula, L_1 and L_2 are the set of planes; k is the threshold; HB_t is the height of the data point in the HB region.

The least square fitting plane of all data points in the set is L_1 , $a_1x + b_1y + c_1z + d_1 = 0$. There are two points, $HB_p(i, j)$. Distances from points to the plane are:

$$d_p(i, j) = \frac{|a_1 i + b_1 j + c_1 HB_p(i, j) + d_1|}{\sqrt{a_1^2 + b_1^2 + c_1^2}} \tag{15}$$

In the formula, $p = 1, 2$. Similarly, distances from points of another set to the plane can also be obtained by the above method. After two projections, the area where the part is not affected by the shadow is *HB*, and the reconstructed contour can be expressed as:

$$HB(i, j) = \{d_p(i, j)\}_{\min} \tag{16}$$

The three-dimensional shape of the reconstructed can be expressed as:

$$H(i, j) = HA_1(i, j) + HA_2(i, j) + HB(i, j) \tag{17}$$

The detection results of the hole obtained by the method of this paper are shown in Fig. 11. Fig. 12 is a comparison of a cross-sectional detection result of the single projector detection method and method proposed in this paper. Where a represents the reconstruction result of the single projector detection method, and b represents the detection result of the proposed method. The X-axis represents the length of the 3d reconstructed part, the Y-axis represents the height.

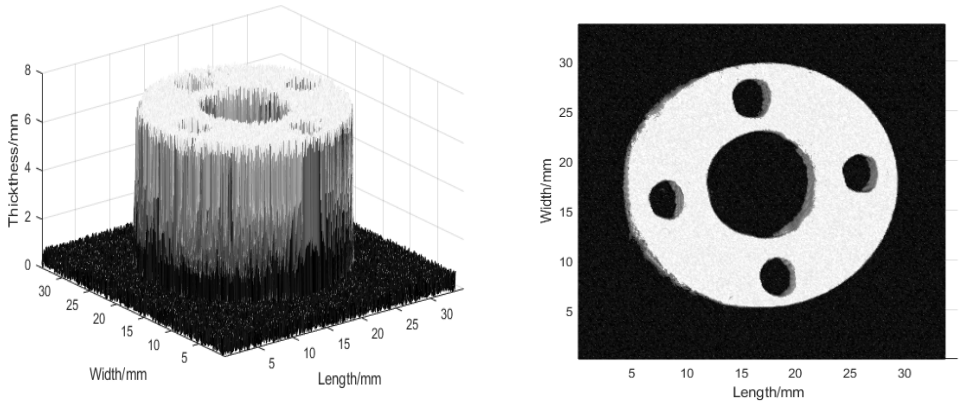

(a) Three-dimensional shape (b) Surface topography

FIGURE 9. The hole reconstructed by the method of single projector.

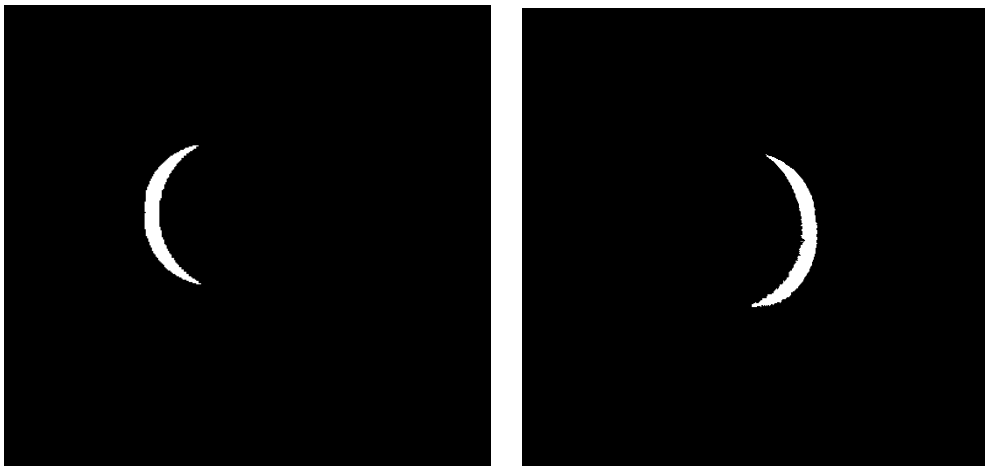

(a)On the left (b)On the right

FIGURE 10. Location of the shaded area.

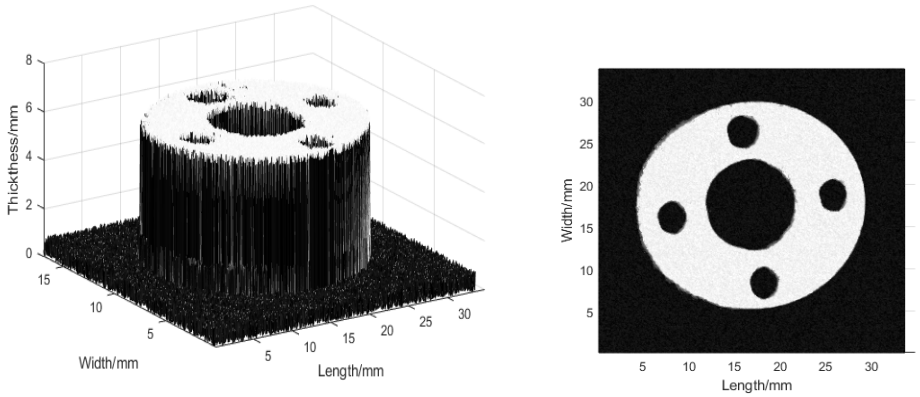

(a) Three-dimensional shape (b) Surface topography

FIGURE 11. The hole reconstructed by the method of this paper.

According to the comprehensive experimental results, the detection method proposed in this paper can reconstruct the shadow region topography more accurately than the single projection detection method.

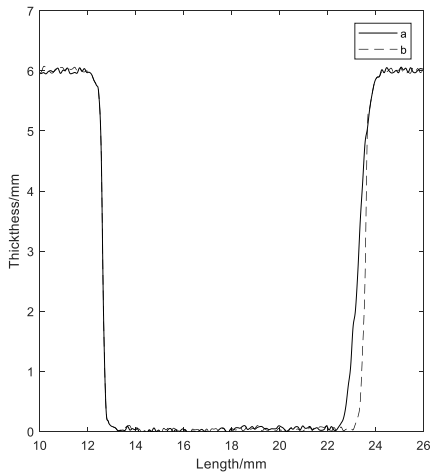

FIGURE 12. The hole reconstructed by the method of this paper.

VI. CALCULATION OF HOLE GEOMETRY SIZE

After completing the 3D reconstruction of the part, it can be found that the reconstructed data is only two planes. The paper sets the height threshold K to split the plane data, and then constructs a bitmap to get the hole plane location map. The edge point of the hole is obtained by the morphological operator, and the geometric size of the hole is obtained by the least square method. Due to the system design, the bottom surface of the part is the reference plane. This plane must be represented as $h = h_0$. In order to improve the calculation efficiency, the bitmap of the hole plane is constructed by the following formula. If $H(i, j)$ is higher than k, set $I(i, j)$ to 0, otherwise set $I(i, j)$ to 1.

$$\begin{cases} I(i,j) = 0, & H(i,j) > k \\ I(i,j) = 1, & H(i,j) \le k \end{cases} \tag{18}$$

K is taken as 0.15mm in this paper, and the constructed bitmap is as follows:

The paper uses the following morphological formula to obtain the hole edge points, and uses the least square method to fit the circle to calculate the geometric information of the hole.

$$G(X) = X - X\Theta g \tag{19}$$

X is the image data to be processed. g is a morphological structural element, which is a 3 * 3 structural element. Θ is an erosion operation. As shown in figure 14, the diameter of a circle is obtained by fitting the circle with the least square method. The hole diameter of the part measured by this method is 19.91mm, and the measurement result by the single projection method is 19.76mm. Compared with the detection results, the method used in this paper improves the detection accuracy of 0.15mm for the measured part hole size.

VII. ANALYSIS OF EXPERIMENTAL RESULTS

In order to verify the accuracy of the method for part thickness measurement, the standard stainless steel block gauge (40mm*30mm*3mm) is tested as shown in Figure 10. The phase measurement profilometry used in this paper measurement results and the wavelet transform profilometry [1] measurement results can be displayed.

Five different gauge block samples were tested. The measurement results are shown in table 1. Table 1 is the comparison between the measurement results of block gauge thickness based on phase measurement profilometry proposed in this paper and the measurement results based on wavelet transform profilometry. The measured maximum and minimum thicknesses of the standard block gauge are extracted as the range of block gauge thickness to be detected. The deviation between the maximum value of the test result and the actual thickness of the block gauge plus the deviation of the minimum value from the actual thickness is the detection accuracy.

Comparison of the diameter measurements of different hole in the part is shown in Table 2. The first column of data is the measurement result of the single-projection measurement

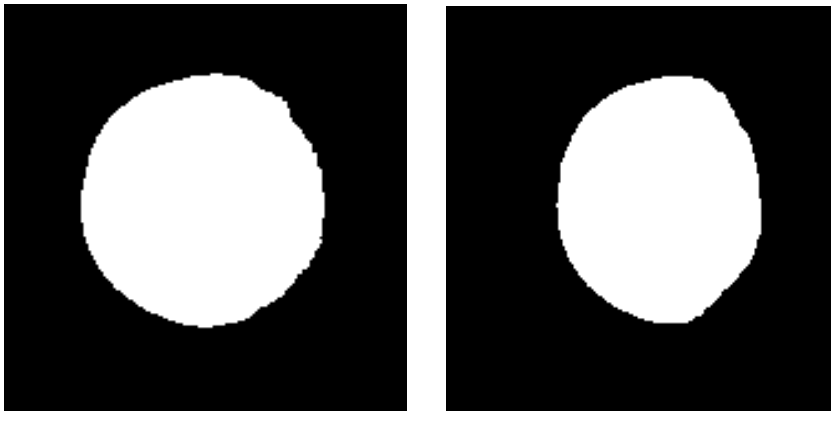

(a) the method of this paper (b) the method of single projection

FIGURE 13. Bitmap of holes.

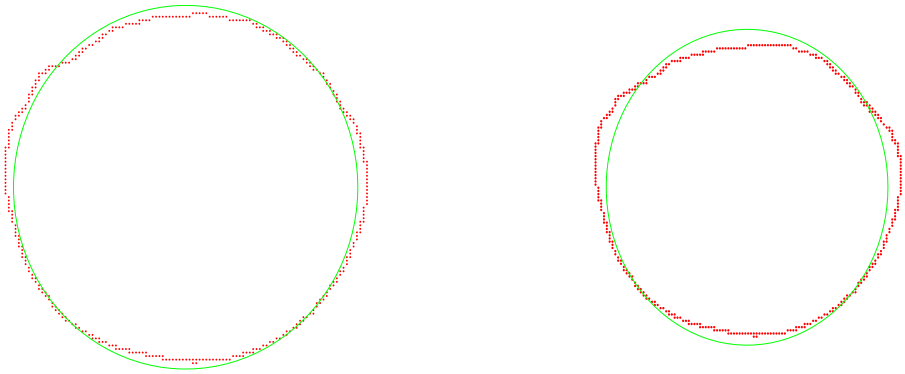

(a) measurement results by the method of this paper

(b) measurement results by the wavelet transform profilometry

FIGURE 14. Calculation of hole size.

TABLE 1. The thickness measurement results of the two methods.

The sample thickness/mm	The measurement results of wavelet transform profilometry/mm			Method measurement results in the paper/mm		
	max	min	error	max	min	error
3	3.04	2.97	0.07	3.02	2.98	0.04
5	5.03	4.98	0.05	5.02	4.98	0.04
7	7.03	6.97	0.06	7.01	6.98	0.03
9	9.04	8.96	0.08	9.02	8.99	0.03
11	11.04	10.98	0.06	11.02	10.98	0.04

TABLE 2. The hole measurement results of the two methods.

The diameter of the hole in the part /mm	The measurement results of single projection/mm	Method measurement results in the paper/mm
7	6.75	6.92
8	7.72	7.91
9	8.70	8.94
10	9.76	9.91
11	10.78	10.92
12	11.71	11.95
13	12.76	12.93
14	13.73	13.92
15	14.75	14.90
16	15.76	15.94

system for the hole of the part, and the second column of data is the measurement result of the method proposed in the paper.

As the experimental results shown in table 1, the measurement accuracy of the plate thickness based on the wavelet transform profilometry is 0.08mm, and the measurement

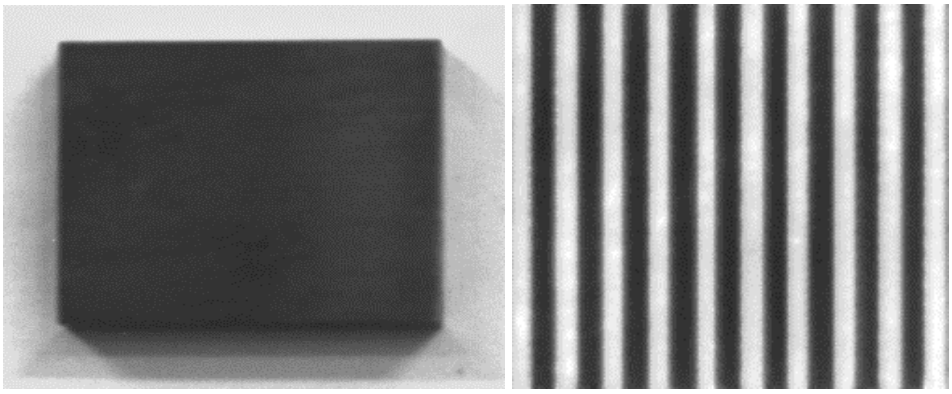

(a) measured gauge block

(b) grating image on the surface

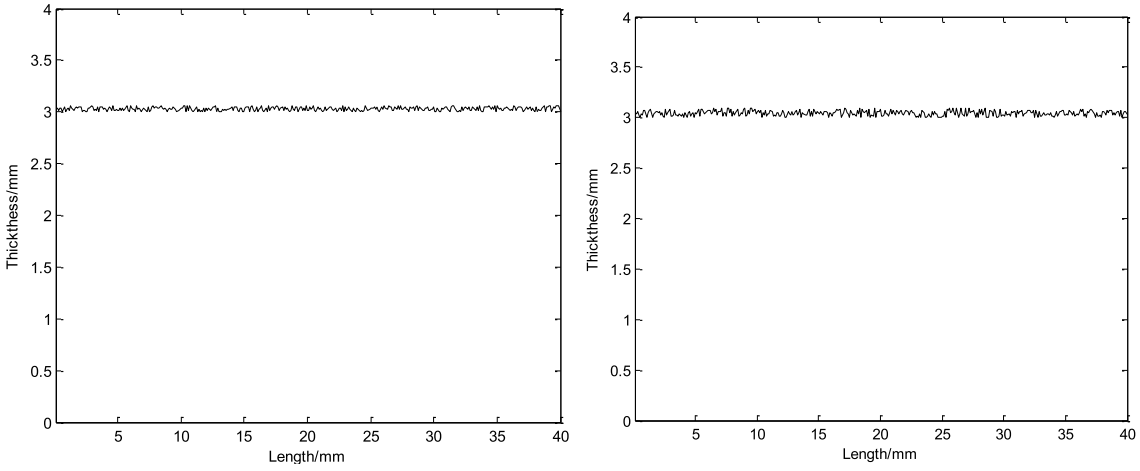

(c) measurement results by the method of this paper

(d) measurement results by the wavelet transform profilometry

FIGURE 15. **Block gauge measurement result.**

accuracy of the proposed measurement method in this paper is 0.04mm. Meanwhile, the experiment results in Table 2 show that the measurement accuracy of the diameter of the hole is lower 0.3 mm and 0.1 mm which used the single-projection measurement system and the proposed method respectively. In summary, the accuracy of the proposed method on the steel thickness detection is 0.04 mm higher than the wavelet transform profilometry, and the measurement error of the hole is reduced by 0.2mm compared with the single projector detection method.

VIII. CONCLUSION

According to the existing quality inspection system, this paper proposes a novel method for detecting the hole of part based on double projection. Compared with the existing quality testing methods, the method proposed in this paper can more accurately reconstruct the three-dimensional shape of the part surface thickness and hole. Firstly, the fringe images of the surface of the part are collected from the two directions by the double projection method. In addition, the fringe image is rectified based on cosine curve, and the surface contour of the part is reconstructed by phase-shift method, and the contour is fused to complete the accurate three-dimensional reconstruction of the hole in the part. Finally, the hole edge feature points are calculated by the morphological formula, so as to obtain the geometric size of the hole in the part. It has been proved by experiments that the accuracy of the method for detecting the thickness of the steel plate can reach 0.04 mm, and the dimensional accuracy of the detection hole can reach 0.1 mm. In this paper, the detection method is better than the existing quality inspection method for the measurement accuracy of part thickness and hole, which meets the requirements of general industrial applications.

REFERENCES

[1] Z. Liu, Y. Jin, J. Wu, and L. Dong, "The online measurement of appearance quality for stainless steel plates based on grating projections," *Insight*, vol. 60, no. 5, pp. 257–263, May 2018.

[2] S. He, J. Li, X. Gao, and L. Luo, "Application of FTP in flaw detection of rail Web," *Optik*, vol. 126, no. 2, pp. 187–190, Jan. 2015.
[3] J.-I. Li, P. Luo, S.-X. He, X.-R. Gao, and L. Luo, "Application of FTP in rail profile and surface flaw detection based on orthogonal two-frequency composite grating," in *Proc. Far East NDT New Technol. Appl. Forum (FENDT)*, Jun. 2017, pp. 318–322.
[4] Y. Jin, Z. Wang, L. Zhu, J. Yang, and B. Wei, "Study on glass defect inspection based on projecting grating method," *J. Test. Eval.*, vol. 41, no. 2, Mar. 2013, Art. no. 20120008.
[5] Y. Zhang, J.-Y. Hu, J.-L. Li, J.-L. Wu, and H.-Q. Wang, "The application of WTP in 3-D reconstruction of train wheel surface and tread defect," *Optik*, vol. 131, pp. 749–753, Feb. 2017.
[6] Y. Zhang, R. Chen, and J. Hu, "Comparative study on three-dimensional reconstruction of wheel surface by FTP and WTP methods," *RISTI*. vol. 15, pp. 181–193, Oct. 2016.
[7] S. Rapuano and F. Harris, "An introduction to FFT and time domain windows," *IEEE Instrum. Meas. Mag.*, vol. 10, no. 6, pp. 32–44, Dec. 2007.
[8] Y. Qian, Y. Li, H. Wang, and F. Hu, "Efficient approach for three-dimensional shape measurement using fringe projection by complex coefficient FIR band-pass filter," *Optik*, vol. 124, no. 5, pp. 456–460, Mar. 2013.
[9] H. Yun, B. Li, and S. Zhang, "Pixel-by-pixel absolute three-dimensional shape measurement with modified Fourier transform profilometry," *Appl. Opt.*, vol. 56, no. 5, p. 1472, Feb. 2017.
[10] T.-W. Hui and G. K.-H. Pang, "3D profile reconstruction of solder paste based on phase shift profilometry," in *Proc. 5th IEEE Int. Conf. Ind. Informat.*, Jul. 2007, pp. 165–170.
[11] T.-W. Hui and G. K.-H. Pang, "3-D measurement of solder paste using two-step phase shift profilometry," *IEEE Trans. Electron. Packag. Manufact.*, vol. 31, no. 4, pp. 306–315, Oct. 2008.
[12] L. Jinlong, D. Fan, L. Lin, and G. Xiaorong, "Wheel profile and tread surface defect detection based on phase measuring profilometry," in *Proc. 18th Int. Wheelset Congr. (IWC)*, Nov. 2016, pp. 71–75.
[13] J. Bruning, "Digital wavefront measuring interferometer for testing optical surfaces and lenses," *Appl. Opt.*, vol. 13, no. 11, pp. 2693–2703, 1974.
[14] C. Ai and J. Wyant, "Effect of piezoelectric transducer nonlinearity on phase shiftinterferometry," *Appl. Opt.*, vol. 26, no. 6, pp. 1112–1116, 1987.
[15] Y. Surrel, "Phase stepping: A new self-calibrating algorithm," *Appl. Opt.*, vol. 32, no. 19, pp. 3598–3600, 1993.
[16] Q. Kemao, S. Fangjun, and W. Xiaoping, "Determination of the best phase step of the Carré algorithm in phase shifting interferometry," *Meas. Sci. Technol.*, vol. 11, no. 8, pp. 1220–1230, 2000.
[17] L. Su, W. Li, and X. Su, "Phase-shift error calibration in modulation measurement profilometry," *Proc. SPIE Int. Soc. Opt. Eng.*, vol. 3749, pp. 546–547, Jul. 1999.
[18] Y. Surrel, "Design of algorithms for phase measurements by the use of phase stepping," *Appl. Opt.*, vol. 35, no. 1, pp. 51–60, 1996.
[19] Y. Fu and Q. Luo, "Fringe projection profilometry based on a novel phase shift method," *Opt. Express*, vol. 19, no. 22, p. 21739, Oct. 2011.
[20] M. Dai, F. Yang, and X. He, "Single-shot color fringe projection for three-dimensional shape measurement of objects with discontinuities," *Appl. Opt.*, vol. 51, no. 12, p. 2062, Apr. 2012.
[21] F. Duan, N. Lv, X. Lou, and P. Sun, "3D profile measurement using heterodyne dual-frequency phase shift method," in *Proc. 6th Int. Symp. Precis. Eng. Meas. Instrum.*, Aug. 2010, Art. no. 75444X.

YONG JIN received the Ph.D. degree from the North University of China, in 2013. He is currently a Professor with the School of Information and Communication Engineering, North University of China. His research interests include the areas of image processing, online inspections, and big data analytics.

YIMIN CHANG is currently pursuing the master's degree with the School of Information and Communication Engineering, North University of China. His research interest includes machine vision.

JIAYING WANG is currently pursuing the master's degree with the School of Electrical Engineering and Telecommunications, University of New South Wales. Her research interests include the fields of image processing and optical fiber communications.

MAOZHEN LI received the Ph.D. from the Institute of Software, Chinese Academy of Sciences, in 1997. He is currently a Professor with the Department of Electronic and Computer Engineering, Brunel University London, U.K. He has over 180 research publications in his research areas including four books. He has served over 30 IEEE conferences. His main research interests include high performance computing, big data analytics and intelligent systems with applications to smart grids, smart manufacturing, and smart cities. He is a Fellow of the British Computer Society and the IET. He serves on the editorial board of a number of journals.

LIHENG REN is currently pursuing the master's degree with the School of Information and Communication Engineering, North University of China. Her research interest includes machine vision.

YOUXING CHEN received the Ph.D. degree from the North University of China, in 2010. He is currently a Professor with the School of Information and Communication Engineering, North University of China. His research interests include the areas of image processing, signal processing, and non-destructive testing.